Geophysical Research Letters

RESEARCH LETTER
10.1029/2021GL096862

Interseismic Strain Accumulation Near Lisbon (Portugal) From Space Geodesy

J. F. B. D. Fonseca[1], M. Palano[2], A. P. Falcão[3], A. Hrysiewicz[4], and J. Fernández[5]

[1]CERENA, Instituto Superior Técnico, Universidade de Lisboa, Lisboa, Portugal, [2]Instituto Nazionale di Geofisica e Vulcanologia, Osservatorio Etneo - Sezone di Catania, Catania, Italy, [3]CERIS, Instituto Superior Técnico, Universidade de Lisboa, Lisboa, Portugal, [4]UCD School of Earth Sciences, University College Dublin, Dublin, Ireland, [5]Institute of Geosciences (CSIC-UCM), Ciudad Universitaria, Madrid, Spain

Key Points:

- We present a GNSS velocity model for the southern Lusitanian Basin and Lower Tagus and Sado Basin
- We complement those results with PSInSAR-derived velocities for the Lisbon Metropolitan Area
- The area in under sinistral simple shear, with velocities and strain-rates pointing to higher seismic hazard than previously estimated

Supporting Information:

Supporting Information may be found in the online version of this article.

Correspondence to:

J. F. B. D. Fonseca,
jfonseca@tecnico.ulisboa.pt

Citation:

Fonseca, J. F. B. D., Palano, M., Falcão, A. P., Hrysiewicz, A., & Fernández, J. (2021). Interseismic strain accumulation near Lisbon (Portugal) from space geodesy. *Geophysical Research Letters*, *48*, e2021GL096862. https://doi.org/10.1029/2021GL096862

Received 4 NOV 2021
Accepted 6 DEC 2021

Abstract The Lisbon Metropolitan Area, Portugal, has been affected by several destructive earthquakes nucleating both along the offshore Africa-Eurasia plate boundary and on onshore inherited intraplate faults. Using a dense GNSS dataset coupled with PSInSAR analysis, we provide new evidence of sinistral simple shear driven by a NNE-SSW first-order tectonic lineament. PSInSAR vertical velocities corroborate qualitatively the GNSS strain-rate field, showing uplift/subsidence where the GNSS data indicate contraction/extension. We propose the presence of a small block to the W of Lisbon moving independently toward the SW with a relative velocity of 0.96 ± 0.20 mm/yr, whose boundaries are part of a complex and as yet poorly constrained strike-slip fault system, possibly rooting at depth into a simpler basement fault. Comparison between geodetic and seismic moment-rates indicates a high seismic coupling. We show that the contribution of intraplate faults to the seismic hazard in the LMA is more important than currently assumed.

Plain Language Summary Satellite data allow for the detection and characterization of surface deformation when points at the Earth's surface move with velocities of the order of 1 mm per year or higher. Using 15-year long series of GNSS observations and 6-year long series of RADAR images from ESA's Sentinel-1 satellites, we characterize the deformation of the Lisbon Metropolitan Area. We conclude that the crust is being stretched in a NE-SW direction, and on top of this pattern we detect a local patch of contraction, near the Tagus river bar. We propose that two blocks of crust are sliding horizontally past each other along the Lower Tagus Valley, inducing a style of deformation in the sediment cover called simple shear, while a smaller block between Lisbon and Cascais moves independently. Our results indicate that the faults near Lisbon contribute more to the seismic hazard of the region then assumed in previous studies, with implications for the building regulations.

1. Introduction

The southern sector of the Lusitanian basin, SW Portugal (Figure 1a), has been the locus of relevant seismicity in historical time (Moreira, 1989; Stucchi et al., 2013). The list of known destructive earthquakes affecting the region and the adjacent continental shelf ranges in time from 1344 to 1909, with catastrophic occurrences in 1356, 1531, and 1755 (https://www.emidius.eu/SHEEC). The existence of important seismogenic structures offshore SW Portugal was recognized at an early stage, but the 1909 earthquake, with epicenter ~40 km to the NE of Lisbon and estimated magnitude in the range M6.0–M6.5, had a clear intraplate nature, and it is widely accepted that the M7 1531 earthquake also nucleated onshore, in the active structures of the Lower Tagus Valley (Canora et al., 2021; Justo & Salwa, 1998). All these features point toward a diffuse zone of deformation involving both onshore and offshore active structures, which accommodate the Nubia-Eurasia plate convergence through a relevant seismicity release, as recently proposed by Palano et al. (2015). The relative importance of the contributions of onshore versus offshore sources to seismic hazard in Portugal is largely debated. On one hand, in view of the modest NW Africa–SW Iberia convergence rate (~4 mm/yr in a NW–SE direction; Fernandes et al., 2003), it has been argued that most of the cumulated crustal deformation is fully released by 1969-type offshore earthquakes of the Gulf of Cadiz, implying that intraplate faults account for very small slip-rates. It follows that destructive intraplate earthquakes are deemed very rare events with limited contribution to the probabilistic hazard (e.g., Ramalho et al., 2020). This view is supported by very low intraplate slip-rate estimates derived from geological studies (0.005–0.3–0.5 mm/yr; Cabral, 2012). On the other hand, seismic hazard disaggregation studies have led

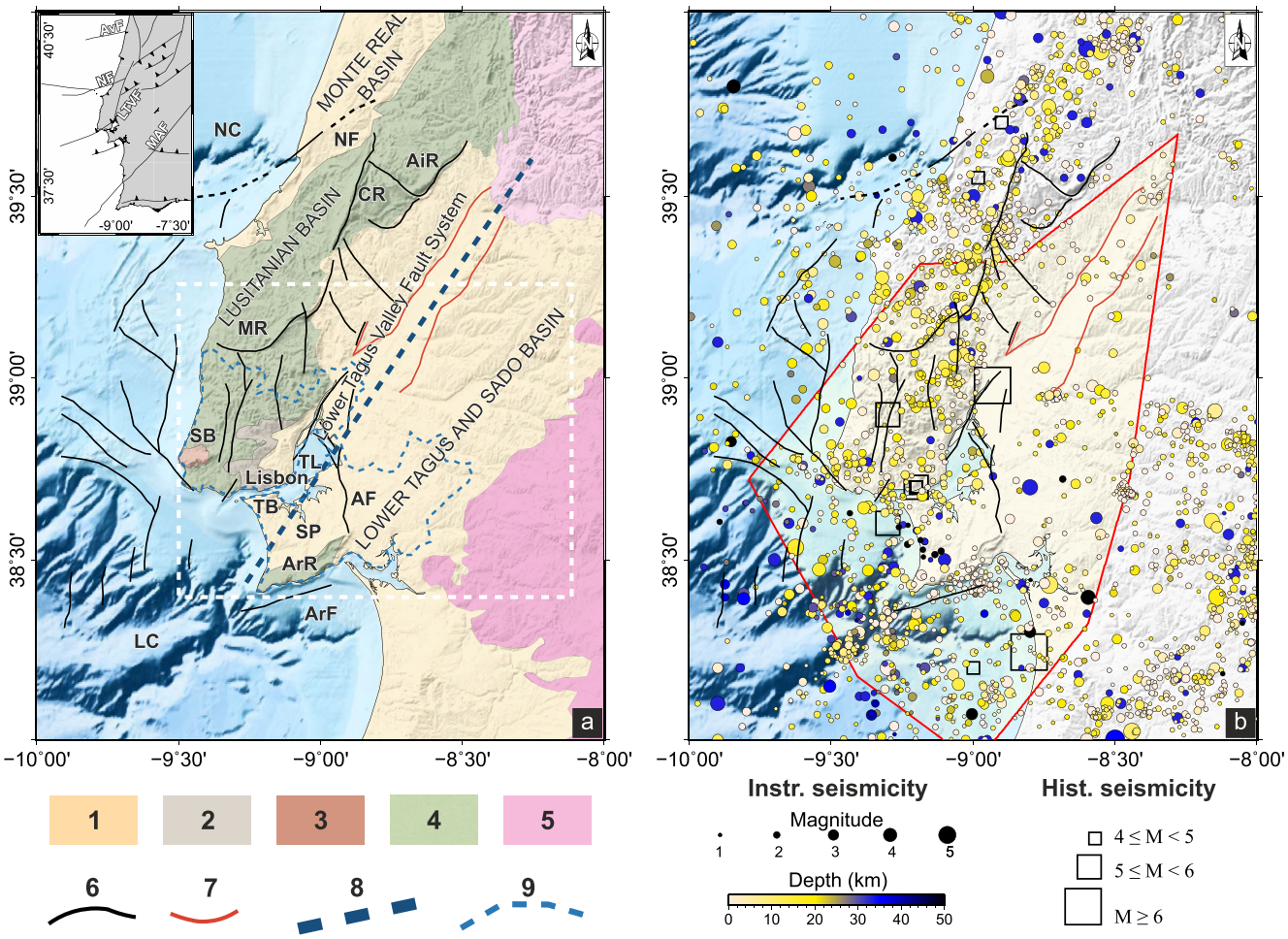

Figure 1. (a) Simplified geology of the Lusitanian Basin and adjacent Cenozoic basins, after the 1:1,000,000 Geological Map of Portugal (LNEG, 2010). Faults (black lines) after Walker (1982), Dickson (1992), and Curtis (1999). Holocene ruptures (red lines) after Canora et al. (2021). The dashed white rectangle delimits the study area. Numbers in legend are: (1) Cenozoic sediments, (2) Lisbon Volcanic Complex, (3) Sintra batholith, (4) Mesozoic sediments, (5) Paleozoic basement, (6) generic fault, (7) fault with Holocene activity, (8) inferred basement fault (Lower Tagus Valley Fault), (9) limits of the Lisbon Metropolitan Area. Abbreviations are: AvF, Aveiro fault; NF, Nazaré fault; LTVF, Lower Tagus Valley fault; MAF, Messejana-Ávila fault; AF, Alcochete fault; AiR, Aire Range; NC, Nazaré Canyon; CR, Candeerios Range; MR, Montejunto Range; SB, Sintra batholith; TL, Tagus lagoon; TB, Tagus bar; SP, Setúbal Peninsula, ArR, Arrábida Range; ArF, Arrábida fault. (b) Seismicity of the study area and surrounding region. Instrumental seismicity (1964–2020) from the International Seismological Center (http://www.isc.ac.uk). Historical seismicity after the SHEEC catalog (Stucchi et al., 2013). The yellow polygon represents the area used for moment rate comparisons.

to opposite conclusions, whereby the rupture of a nearby intraplate fault is the dominant scenario (Vilanova & Fonseca, 2007; Woessner et al., 2015).

Space geodesy may hold the key to arbitrate this issue, since it allows the direct observation and quantification of interseismic strain buildup (Bennett et al., 1998; Murray et al., 2014; Lange et al., 2019). The southern Lusitanian basin hosts a significant number of GNSS stations at an average spacing of ~30 km, continuously operating in the last 15 years. To constrain both intraplate deformation style and rates of the southern sector of the Lusitanian basin, we used the available GNSS data. In addition, PSInSAR (Persistent Scatterer Interferometry of Synthetic Aperture RADAR) analysis, which has complementary characteristics to GNSS (Farolfi et al., 2019), was used to characterize further the vertical and East-West components of motion, with increased spatial resolution.

2. Regional Tectonics

The Lisbon Metropolitan Area (LMA; Figure 1a) is located on the southern sector of the Lusitanian Basin (LB) in the western coast of Iberia, a rift margin that formed ~200 million years ago when the North Atlantic rift system incised the Paleozoic crust of the Hesperic Massif (Wilson et al., 1989; Rasmussen et al., 1988). The LB

early formation was controlled by a set of crustal-scale strike-slip faults (Aveiro fault, Nazaré fault, Lower Tagus Valley fault, Messejana-Ávila fault) inherited from the Hercynian Orogeny (Arthaud & Matte, 1977; Pereira & Alves, 2013; Pinheiro et al., 1996). The study area straddles one of these Hercynian crustal fractures, the Lower Tagus Valley fault (LTVF). Triassic and Early Jurassic deposits comprise important amounts of evaporites, which accumulated in grabens and half-grabens at depths ranging from 2 to 4.5 km and thicknesses from 200 to 1500 m (Rasmussen et al., 1998; Reis et al., 2017). With the onset of seafloor spreading, the LB became an aborted rift (Hubbard, 1988), and halokinesis played an important role in its evolution, with different sectors developing independently as fault-bounded or salt-wall bounded sub-basins (Alves et al., 2003; Montenat et al., 1988. The main faults through the sediment fill of the LB revealed by commercial seismic reflection data (Walker, 1982) are depicted in Figure 1a. During the Alpine Orogeny the LB underwent structural inversion (Curtis, 1999), which stops abruptly at the ENE-WSW Arrabida range, the southern limit of the LB (A. F. Fonseca et al., 2020). Palaeoseismological and geomorphological investigations have unveiled Holocene ruptures on two parallel strands of faults along the Tagus River (Figure 1a) in response to the current stress field, characterized by a NW-SE maximum compressive stress (Ribeiro et al., 1996), with geomorphic indicators of sinistral strike-slip (Canora et al., 2015, 2021; Ostman et al., 2012). The southern sector of the LB hosts significant historical seismicity (Moreira, 1989; Stucchi et al., 2013), but during the last decades, the region has experienced quiescence (Custodio et al., 2015), with only $M < 3$ earthquakes that form a diffuse pattern (Figure 1b).

3. Data and Methods

A total of 22 continuous GNSS stations covering the study area were processed using the GAMIT/GLOBK 10.71 software (Herring, 2003; http://www-gpsg.mit.edu), adopting the strategy described in the Supplementary Information. To improve the overall configuration of the network and tie the regional measurements to an external global reference frame, data coming from additional 117 continuously operating global tracking stations were also introduced in the processing (Figure S1 in Supporting Information S1). To adequately show the crustal deformation pattern over the investigated area, the GNSS velocity field was aligned to a fixed Eurasian reference frame (Altamimi et al., 2016). The resulting horizontal and vertical velocities are shown in Figure 2a).

Vertical and East–West velocities relative to a pair of reference points were also computed using 311 ascending-orbit and 306 descending-orbit Sentinel-1 Synthetic Aperture Radar images (Burgmann et al., 2000) acquired between 2014 and 2020, with the PSInSAR technique (Ferretti et al., 2000), using the GAMMA software (Wegmuller et al., 2019; Werner et al., 2000). These results are independent from the GNSS velocity estimates and have a much higher spatial resolution. Colocated (within 50m) GNSS and PSInSAR observations were used to remove the effect of the motion of reference points. Figure 3 displays the estimated velocities after conversion to the GNSS reference frame. See the Supporting Information for additional details.

4. Results

Velocities with respect to stable Eurasia for 22 GNSS stations on the LB and on the adjacent LTSB are reported in Figure 2a. In general, the stations move toward the NW quadrant with an average velocity of ∼1.5 mm/yr. We selected for further analysis a subset of 12 stations located on the LMA (see the red dashed rectangle in Figure 2a). In order to filter out localized deformations of possible geotechnical origin, we compared each horizontal velocity with the average of the four nearest sites. We excluded the IGEO station (Figure 2b) from the analysis because its motion deviates significantly from the neighbor stations. To the West of the Tagus estuary, a few other sites show significant deviations but in a coherent pattern. The average velocity of the three stations with green arrows with respect to the average velocity of the remaining eight sites of the study area (red-dashed rectangle) is 0.96 ± 0.20 mm/yr, with an azimuth of ∼217° (red arrow in Figure 2a). Station CASC moves differently from those immediately to its East but according to the average velocity of the region. Because station CASC has a robust monument and a long history of observation (1997 to present), we accept its velocity as a reliable result. The significance of these anomalous velocities will be discussed below.

The GNSS-based vertical velocities (Figure 2a) depict a general subsidence pattern with rates up to ∼1.5 mm/yr, mainly located along the Lower Tagus valley. However, vertical velocities are not as coherent at the submillimeter/yr level as the horizontal components (Figure 2a), due to local processes that may affect motions and uncertainties; therefore, we focus on the vertical velocities coming from PSInSAR analysis.

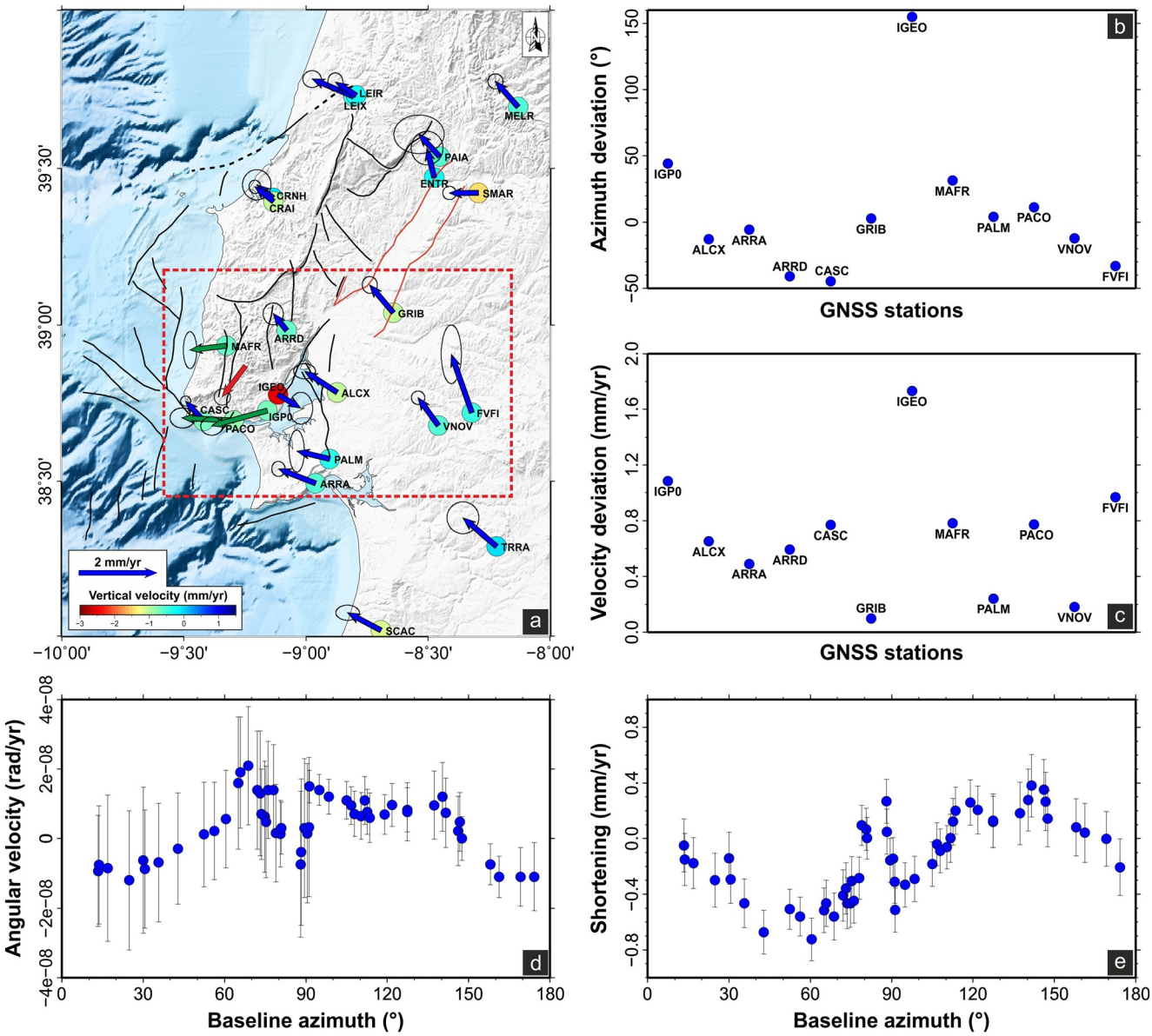

Figure 2. (a) GNSS-derived velocities with respect to stable Eurasia. Arrows represent horizontal velocities, and ellipses show the 95% confidence interval. Vertical velocities are reported as colored points. Stations located in the red-dashed rectangle were analyzed to remove local deformations (see the main text for details). The red arrow is the average velocity of the sites colored in green relative to the average velocity at the remaining stations. (b) Deviation of the azimuth of velocity of each site with respect to the average velocity of the four nearest sites. (c) Deviation of the scalar velocity of each site with respect to the average of the four nearest sites. (d) Baseline rotation as a function of azimuth. Positive angular velocities correspond to counterclockwise rotation. (e) Baseline shortening/extension as a function of azimuth. Positive values correspond to shortening. Azimuths are clockwise from North.

Figure 3a shows the vertical velocities inferred from the PSInSAR analysis using ascending and descending orbits, ranging from 3 ± 1 mm/yr of subsidence to 1 ± 1 mm/yr of uplift (after correction to the same reference frame adopted for the GNSS-derived velocities, see Supporting Information for details and PSInSAR-GNSS velocity correlation plots). We are assigning an uncertainty of ± 1 mm/yr to all PRInSAR-derived components of velocity. Subsidence is dominant near the margins of the Tagus river, on the eastern Setubal peninsula and in the vicinity of the Arrabida range, displaying a close association with the faults that cut through the post-Oligocene sediments of the LTSB (black lines in Figure 3). A zone of uplift (or absence of subsidence) can be observed to the SW of the city of Lisbon. The East–West velocity field depicted in Figure 3b shows good agreement with the same velocity component inferred from GNSS. It lends some support to the southeastward motion of GNSS site

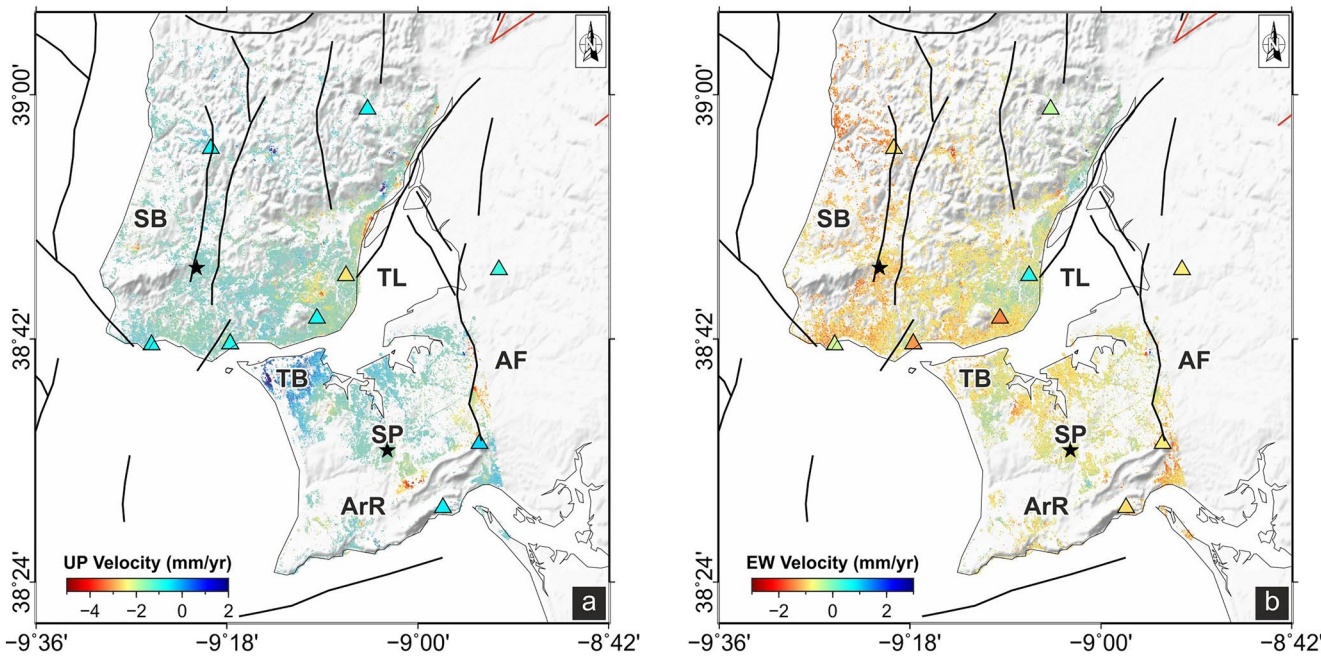

Figure 3. (a) InSAR vertical velocities in the study area (89,988 points), derived from Sentinel-1 images. Positive velocities (cold colors) correspond to uplift, negative velocities (warm colors) correspond to subsidence. The velocities were computed in relation to two reference points (one per margin; black stars), and then converted to the GNSS reference frame (see the Supporting Information for details). Black lines depict faults through the sediments. Abbreviations are as in Figure 1. (b) The same for East-West velocities. Cold (warm) colors for eastward (westward) movement.

IGEO, which may afterall have a tectonic rather than geotechnical origin. However, this interpretation must be taken with caution given the uncertainty of the velocity estimates.

Finally, Figure 4 depicts the horizontal strain-rates (and associated uncertainties) estimated on a regular $0.1° \times 0.1°$ grid over the investigated area by adopting the method reported in Shen et al. (2015). The results are unreliable in both the northenmost and the southernmost sectors of the study region (uncertainties larger than the strain-rate values). Regarding the Lower Tagus Valley and the surrounding area the strain-rate estimates are reliable, especially on the extensional components. Here, the strain-rate is characterized by a sharp extension of ∼15 nstrain/yr with NE–SW axis coupled with a small contraction (3–4 nstrain/yr) in the NW–SE direction. A local patch of reliable contraction (∼15 nstrain/yr) can be observed close to the Lisbon-Tagus bar region, with the shortening axis oriented NNE–SSW.

5. Discussion

5.1. Active Tectonics of the LMA

A first-order observation, according to the horizontal strain-rate field (Figure 4a), is that the crust of the LMA is experiencing NE–SW extension, except in the zone around the Tagus bar and in the western Setubal Peninsula, which display significant NNE-SSW shortening. This is consistent with the PSInSAR estimates of vertical velocity (Figure 3a), showing uplift near the Tagus bar but mostly subsidence elsewhere. This extensional regime is also consistent with the long-term evolution of the Tagus lagoon, the only zone of Portugal to display subsidence during the Quaternary (Cabral, 2012).

Figures 2d and 2e provide further insight into the horizontal deformation pattern. Baselines having the azimuth in the range N30E to N110E undergo predominantly extension (Figure 2e), in agreement with the strain-rate map (Figure 4a). Baselines with azimuth in the range N70 W to N20 W display shortening instead, also consistent with the strain-rate field. Moreover, Figure 2d shows that most baselines rotate counterclockwise, with a few exceptions in the range N30W–N50 E. Taken together, these results are strongly indicative of simple sinistral shear above a strike-slip fault with NNE–SSW orientation, as depicted schematically in Figure 4b. Segments connecting stations with green arrows in Figure 2a tend to have an anomalous behavior, visible near azimuth N85E,

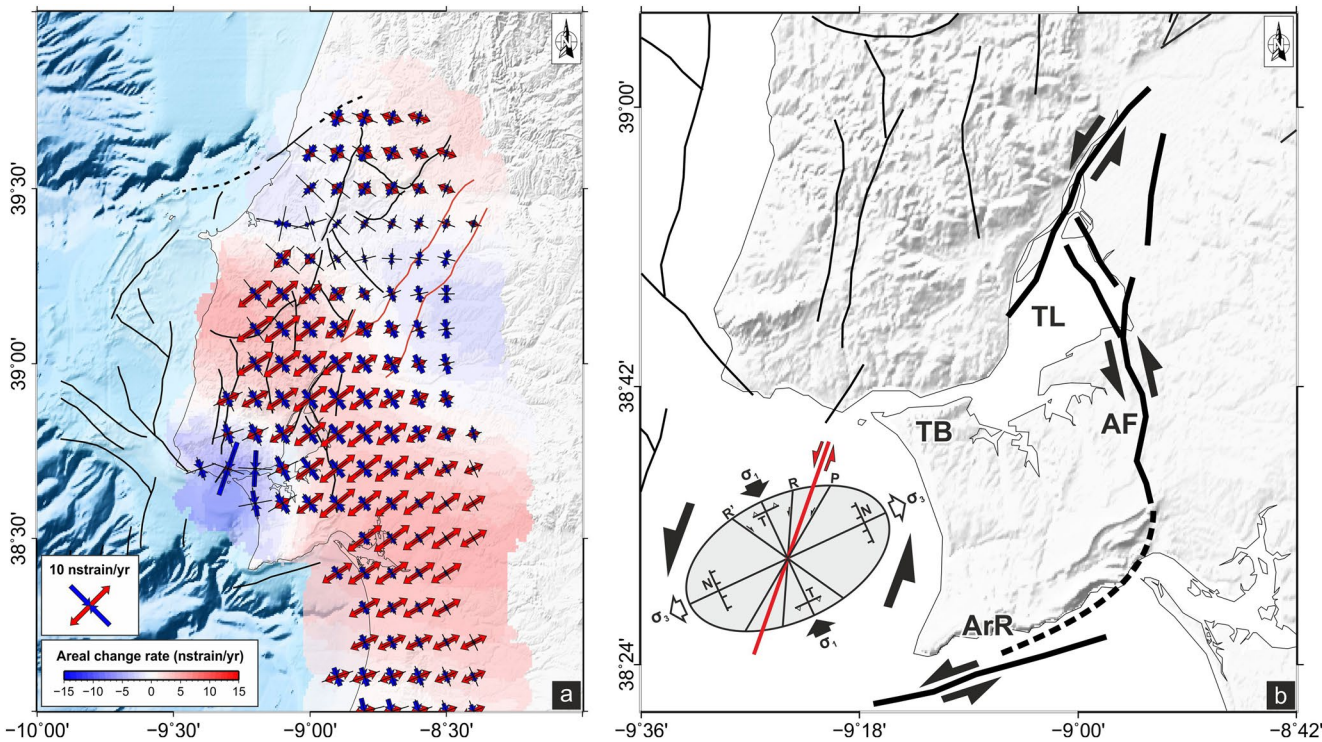

Figure 4. (a) Strain-rates inferred from the GNSS horizontal velocities (see text for details). Blue corresponds to areas under compression, pink to areas under extension. (b) Schematic tectonic interpretation of the study area, after Vilanova and Fonseca (2004). Abbreviations are: AF, Alcochete fault; ArR, Arrábida Range; TL, Tagus lagoon; TB, Tagus bar. Inset: schematic representation of the simple-shear deformation of ductile sediment cover on top of a sinistral strike slip fault. Red line: underlying basement fault; R, synthetic Riedel shear; R', antithetic Riedel shear; N, normal fault, T, thrust and reverse fault; P, secondary synthetic shear; σ_1 and σ_3, principal stress axes. Modified from Sylvester (1988).

showing contraction and rotating clockwise against the dominant tendency. Together with the observation that this group of sites moves with an average velocity of 0.97 ± 0.20 mm/yr toward the SW quadrant with respect to the average velocity of the remaining sites, this behavior indicates the presence of a small crustal block to the W of Lisbon, moving independently, possibly related to a local lateral extrusion process. The contrasting motion of GNSS site IGEO may be related to the eastern boundary of this block. On the western side, it can be speculated that CASC is "pinned" by the Sintra batholith that lays to its north. Paleoseismological and geomorphological investigations are probably the only path to improve our understanding of the active deformation of the region, despite the challenges put by the urban development of the LMA.

A likely explanation for the complex pattern of deformation near Lisbon concerns the connection of the LTVF with the offshore fault system (Figure 1a). As it approaches the broad lagoon of the Tagus estuary, the fault system swings to a N-S direction along the Alcochete fault, in a releasing bend (e.g., Sylvester, 1988) that causes NE–SW extension and subsidence. Figure 3 shows that this subsidence is linked to the activity of the fault system, confirming that the Tagus lagoon is an active pull-apart basin as proposed by Vilanova and Fonseca (2004). When it reaches the S of the Arrabida range, the fault system changes direction again, adopting a ENE–WSW strike and dip-slip motion (Figure 4b), changes of direction and style that configure a single restraining bend (Cunningham & Mann, 2007), explaining the compression and uplift detected in the Setúbal peninsula. Gradients of PSInSAR-derived velocities–both vertical and East–West–in the city of Lisbon, together with the anomalous behavior of GNSS site IGEO, may indicate that the NNE-SSW LTVF extends further to the SW through the city.

Our results do not clarify to what extent this complexity is also present at basement level, given the effective detachment at the base of the sediment fill (Rasmussen et al., 1998; Reis et al., 2017). The uplift/subsidence boundary observed south of the Tagus bar (Figure 3a) is aligned with the trend of the LTVF further to the NE, and this may indicate that at depth the crustal fault continues as a linear feature toward the offshore. Although the tectonic relevance of the canyons has been a topic of speculation for many decades (Pinheiro et al., 1996; Pereira & Alves, 2013), it is a fact that they are aligned with major crustal faults (see inset in Figure 1a) further

north (Nazaré fault) as well as further South (Messejana-Ávila fault). A continuation of the linear trend described above through the continental shelf is therefore supported by its alignment with the Lisbon Canyon (Lastras et al., 2009).

5.2. Moment Rate Estimates

Geodetically derived strain cannot be equated directly to seismic moment release, since a significant percentage of the deformation may be aseismic (e.g., Masson et al., 2005; Palano et al., 2018). Taking as reference the source area used by Woessner et al. (2015) to account for the seismicity of the Lower Tagus Valley (Figure 1b), and using 15 km for seismogenic thickness and *30* GPa for crustal rigidity we estimate a value of $\dot{M}_0^{geod} = 1.35 \times 10^{17}$Nm/yr for the scalar geodetic moment-rate (see the Supporting Information). Ramalho et al. (2020) reviewed the probabilistic seismic hazard assessment of Woessner et al. (2015) and estimated $\dot{M}_0^{seis}$ from the Gutenberg-Richter parameters for the same source area, so a direct comparison between the two results can be performed. For the three values of maximum magnitude (7.1, 7.4, and 7.6) considered by Woessner et al. (2015), Ramalho et al. (2020) obtained $\dot{M}_0^{seis}$ of 8.69×10^{16}, 1.33×10^{17}, and 1.77×10^{17} Nm/yr, respectively. These values compare well with our geodetic estimate of the moment-rate, especially the central value, suggesting a strong seismic coupling of the area.

5.3. Hazard Implications

It is important to confront assumptions regarding seismic hazard with the new results put forward here. Because fault slip-rate $\dot{\boldsymbol{d}}$ is directly linked to seismic moment-rate $\dot{\boldsymbol{M}}_0$ through the fundamental relation $\dot{\boldsymbol{M}}_0 = \boldsymbol{\mu A}\dot{\boldsymbol{d}}$ where $\boldsymbol{\mu}$ is rigidity and $\boldsymbol{A}$ is rupture area, its value imposes a strong constraint on seismic recurrence models, hence on seismic hazard estimates (Anderson & Luco, 1983; Youngs & Coppersmith, 1985). Cabral (2012) state that the intraplate faults of Western Iberia have very slow slip-rates, in the range 0.005 to 0.3–0.5 mm/yr, with return periods larger than 5000 years for $M > 6$ earthquakes, having therefore a small contribution to the hazard at the regulatory return period of 475 years when compared to more distant offshore faults. Our results suggest that those values are exceeded in the vicinity of Lisbon. Although the velocities and rates reported here cannot be directly extrapolated to the basement given the likely detachment at the bottom of the basin fill, our reported block velocity of 0.97 ± 0.20 mm/yr is incompatible with the low intraplate slip-rates that have been assumed in several hazard studies, among which the one at the basis of the EUROCODE 8 National Document for Portugal (Costa et al., 2008). Also, the reported strain-rates, of the order of 15 nstrain/yr or $\sim 5 \times 10^{-16}$ s^{-1}, are higher than those typically associated with intraplate areas (10^{-17} to 10^{-20} s^{-1} according to Molnar, 2020) and are comparable to those observed in the Basin and Range ($\sim 3 \times 10^{-16}$ s^{-1} according to Payne et al., 2008) or in Southern Tibet ($\sim 4 \times 10^{-16}$ s^{-1} according to Wang et al., 2019). Further investigation of the faults of the LMA with the techniques of Active Tectonics and Paleoseismology should therefore be a priority for the improvement of regional seismic hazard assessment.

6. Concluding Remarks

The analysis of GNSS data in the LMA revealed a pattern of interseismic deformation consistent with simple shear on top of a locked strike slip basement fault oriented NNE-SSW, with strain-rates of the order of 15 nstrain/yr, both extensional and contractional. Velocities independently derived from radar images with the PSInSAR technique broadly corroborate these results, showing uplift (subsidence) where the GNSS data detect contraction (extension). A block to the West of Lisbon, sampled by three GNSS sites, moves with respect to the surrounding region on both sides with a relative velocity of 0.96 ± 0.20 mm/yr, possibly as the result of small-scale lateral extrusion. These results support the hypothesis that the Lower Tagus Valley is the locus of an active first-order crustal fault which drives the observed simple shear surface deformation, while contradicting the widespread view (e.g., Ramalho et al., 2020) that the LTV faults are too slow to contribute with a major parcel to the seismic hazard of the region. The impact of intraplate faults in the seismic hazard of the LMA may therefore be more important than currently assumed.

Data Availability Statement

Crustal velocity data and seismicity data used to produce the figures in the study are available at Zenodo via https://doi.org/10.5281/zenodo.5646484 with free access. The raw RINEX data of the SERVIR CORS and Re-NEP networks used in this paper were kindly yielded by the Instituto Geográfico do Exército, Lisbon, and Direcção Geral do Território, Lisbon, respectively. The European Space Agency (ESA) provided Sentinel-1 IW SAR data, and NASA offered the SRTM DEM. Instrumental seismicity data were downloaded from the International Seismological Center (Storchak et al., 2020). Access to the raw RINEX data used to derive GNSS velocities can be requested from snig@dgterritorio.pt and igeoe@igeoe.pt free of charge (registration is required). The SAR images (2014–2020) used to derive the PSInSAR velocities can be downloaded free of charge from https://scihub.copernicus.eu/dhus/#/home (insert "Portugal" as search criteria; after this step registration is required). All figures were prepared with the GMT software (Wessel & Smith, 1991). The raw GNSS data used to derive the velocities used in this paper belong partly to the Portuguese Army (IGEOE-Instituto Geografico do Exercito) and are treated as sensitive under Portuguese law. Any researcher can gain access to the data but, according to the IGEOE guidelines, (s)he needs to register. Note that this restriction applies to the raw RINEX data only, and all the velocities derived from those data were uploaded to the Zenodo repository.

Acknowledgments
J.F.B.D.F. acknowledges support from the Portuguese research foundation FCT, under Line of Excellence grant EXCL/GEO-FIQ/0411/2012 - Seismicity of Plate Interiors: Challenges to Hazard Evaluation. A.P.F. acknowledges support from AGEO—Platform for Atlantic Geohazard Risk Management (https://ageoatlantic.eu/, Grant No. EAPA_884/2018. A.H. acknowledges support from University College, Dublin and iCRAG2, and thanks GAMMA's staff for InSAR support. Research by M.P. and J.F. was supported by the AEI Spanish research project DEEP-MAPS, Grant Agreement No. RTI2018-093874-B-100. This work represents a contribution to CSIC Thematic Interdisciplinary Platform PTI TELEDETECT. The authors are grateful to two anonymous reviewers for their constructive criticisms, which helped improve the manuscript.

References

Altamimi, Z., Rebischung, P., Métivier, L., & Collilieux, X. (2016). ITRF2014: A new release of the International Terrestrial Reference Frame modeling nonlinear station motions. *Journal of Geophysical Research: Solid Earth*, *121*, 6109–6131. https://doi.org/10.1002/2016JB013098

Alves, T. M., Gawthorpe, R. L., Hunt, D. W., & Monteiro, J. H. (2003). Cenozoic tectonosedimentary evolution of the western Iberian margin. *Marine Geology*, *195*, 75–108. https://doi.org/10.1016/S0025-3227(02)00683-7

Anderson, J. G., & Luco, J. E. (1983). Consequences of slip rate constraints on earthquake occurrence relations. *Bulletin of the Seismological Society of America*, *73*, 471–496. https://doi.org/10.1785/bssa0730010045

Arthaud, F., & Matte, P. (1977). Late palaeozoic strike-slip faulting in southern Europe and Northern Africa: Result of a right-lateral shear zone between the Appalachians and the Urals. *The Geological Society of America Bulletin*, *88*, 1305–1320. https://doi.org/10.1130/0016-7606(1977)88<1305:lpsfis>2.0.co;2

Bennett, R. A., Wernicke, B. P., & Davis, J. L. (1998). Continuous GPS measurements of contemporary deformation across the northern Basin and Range province. *Geophysical Research Letters*, *25*(4), 563–566. https://doi.org/10.1029/98gl00128

Burgmann, R., Rosen, P. A., & Fielding, E. J. (2000). Synthetic aperture radar interferometry to measure Earth's surface topography and its deformation. *Annual Review of Earth and Planetary Sciences*, *28*, 169–209. https://doi.org/10.1146/annurev.earth.28.1.169

Cabral, J. (2012). Neotectonics of mainland Portugal: State of the art and future perspectives. *Journal of Iberian Geology*, *38*(1), 71–84. https://doi.org/10.5209/rev_jige.2012.v38.n1.39206

Canora, C., Vilanova, S. P., De Pro-Diáz, Y., Pina, P., & Heleno, S. (2021). Evidence of surface rupture associated with historical earthquakes in the lower Tagus valley, Portugal. Implications for seismic hazard in the Greater Lisbon Area. *Frontiers of Earth Science*, *9*. https://doi.org/10.3389/feart.2021.620778

Canora, C., Vilanova, S. P., Ostman, G. M. B., Carvalho, J., Heleno, S., & Fonseca, J. F. B. D. (2015). The eastern lower Tagus valley fault zone in central Portugal: Active faulting in a low-deformation region within a major river environment. *Tectonophysics*, *660*, 117–131. https://doi.org/10.1016/j.tecto.2015.08.026

Costa, A. C., Sousa, M. L., & Carvalho, A. (2008). Seismic zonation for Portuguese national annex of Eurocode 8. In *Proceedings of the 14th World Conference on Earthquake Engineering*, China.

Cunningham, W. D., & Mann, P. ((2007). Tectonics of strike-slip restraining and releasing bends. In W. D. Cunningham, & P. Mann (Eds.), *Tectonics of strike-slip restraining and releasing bends* (Vol. 290, pp. 1–12). Geological Society, London, Special Publications. https://doi.org/10.1144/sp290.1

Curtis, M. L. (1999). Structural and kinematic evolution of a Miocene to Recent sinistral restraining bend: The Montejunto massif, Portugal. *Journal of Structural Geology*, *21*, 39–54. https://doi.org/10.1016/s0191-8141(98)00095-9

Custódio, S., Dias, N. A., Carrilho, F., Góngora, E., Rio, I., Marreiros, C., et al. (2015). Earthquakes in Western Iberia: Improving the understanding of lithospheric deformation in a slowly deforming region. *Geophysical Journal International*, *203*, 127–145.

Dickson, A. J. (1992). *A regional seismic interpretation of offshore Portugal (M.Sc. Thesis)*. U.K: University of Durham.

Farolfi, G., Piombino, A., & Catani, F. (2019). Fusion of GNSS and satellite radar interferometry: Determination of 3D fine-scale map of present-day surface displacements in Italy as expressions of geodynamic processes. *Remote Sensing*, *11*, 394. https://doi.org/10.3390/rs11040394

Fernandes, R. M. S., Ambrosius, B. A. C., Noomen, R., Bastos, L., Wortel, M. J. R., Spakman, W., & Govers, R. (2003). The relative motion between Africa and Eurasia as derived from ITRF2000 and GPS data. *Geophysical Research Letters*, *30*, 1828–1840. https://doi.org/10.1029/2003gl017089

Ferretti, A., Prati, C., & Rocca, F. (2000). Non-linear subsidence rate estimation using persistent scatterers in differential SAR interferometry. *IEEE Transactions on Geoscience and Remote Sensing*, *38*(5), 2202–2212. https://doi.org/10.1109/36.868878

Fonseca, A. F., Zêzere, J. L., & Neves, M. (2020). The Arrabida Chain: The Alpine Orogeny in the vicvinity of the Atlantic ocean. In G. Vieira, J. L. Zêzere, & C. Mora (Eds.), *Landscapes and Landforms of Portugal, World Geomorphological Landscapes* (pp. 273–278). Springer Nature. https://doi.org/10.1007/978-3-319-03641-0_21

Herring, T. A. (2003). MATLAB Tools for viewing GPS velocities and time series. *GPS Solutions*, *7582*(3), 194–199. https://doi.org/10.1007/s10291-003-0068-0.583

Herring, T. A., King, R. W., Floyd, M. A., & McClusky, S. C. (2018). *Introduction to GAMIT/GLOBK*, Release 10.7. Cambridge, UKMassachusetts Institute of Technology.

Hubbard, R. J. (1988). Age and significance of sequence boundaries on Jurassic and early Cretaceous rifted continental margins. *Bulletin: American Association of Petroleum Geologists*, *72*(1), 49–72. https://doi.org/10.1306/703c81c8-1707-11d7-8645000102c1865d

Justo, J. L., & Salwa, C. (1998). The 1531 Lisbon earthquake. *Bulletin of the Seismological Society of America*, *88*(2), 319–328.
Lange, D., Kopp, H., Royer, J.-Y., Henry, P., Çakir, Z., Petersen, F., et al. (2019). Interseismic strain build-up on the submarine North Anatolian fault offshore Istanbul. *Nature Communications*, *10*, 3006. https://doi.org/10.1038/s41467-019-11016-z
Lastras, G., Arzola, R. G., Masson, D. G., Wynn, R. B., Huvenne, V. A. I., Huhnerbach, V., & Canals, M. (2009). Geomorphology and sedimentary features in the Central Portuguese submarine canyons, western Iberian margin. *Geomorphology*, *103*(3), 310–329. https://doi.org/10.1016/j.geomorph.2008.06.013
Masson, F., Chery, J., Hatzfeld, D., Martinod, J., Vernant, P., Tavakoli, F., & Ghafory-Ashtiani, M. (2005). Seismic versus aseismic deformation in Iran inferred from earthquakes and geodetic data. *Geophysical Journal International*, *160*, 217–226. https://doi.org/10.1111/j.1365-246X.2004.02465.x
Molnar, P. (2020). The brittle-plastic transition, earthquakes, temperatures, and strain-rates. *Journal of Geophysical Research: Solid Earth*, *125*e2019JB019335. https://doi.org/10.1029/2019JB019335
Montenat, C., Guery, F., Jamet, M., & Berthou, Y. B. (1988). Mesozoic evolution of the Lusitanian basin: Comparison with the adjacent margin. In G. Boillot, E. L. Winterer, & A. W. Meyer (Eds.), *Proceedings of the Ocean Drilling Program Scientific Results* (Vol. 103, pp. 757–775). Ocean Drilling Program. https://doi.org/10.2973/odp.proc.sr.103.117.1988
Moreira, V. (1989). Seismicity of the Portuguese continental margin. In S. Gregersen, & P. Basham (Eds.), *Earthquakes at North-Atlantic passive margins: Neotectonics and postglacial rebound* (pp. 533–545). Kluwer Academic Publishers. https://doi.org/10.1007/978-94-009-2311-9_31
Murray, J. R., Minson, S. E., & Svarc, J. L. (2014). Slip rates and spatially variable creep on faults of the northern San Andreas system inferred through Bayesian inversion of Global Positioning System data. *Journal of Geophysical Research: Solid Earth*, *119*, 6023–6047. https://doi.org/10.1002/2014JB010966
Ostman, G. M. B., Vilanova, S. P., Nemser, E. S., Falcao-Flor, A., Heleno, S. I. N., Ferreira, H. E., & Fonseca, J. F. B. D. (2012). Large Holocene earthquakes in the lower Tagus valley fault zone, Central Portugal. *Seismological Research Letters*, *83*, 67–76. https://doi.org/10.1785/gssrl.83.1.67
Palano, M., González, P. J., & Fernández, J. (2015). The diffuse plate boundary of Nubia and Iberia in the Western Mediterranean: Crustal deformation evidence for viscous coupling and fragmented lithosphere. *Earth and Planetary Science Letters*, *430*, 439–447. https://doi.org/10.1016/j.epsl.2015.08.040
Palano, M., Imprescia, P., Agnon, A., & Gresta, S. (2018). An improved evaluation of the seismic/geodetic deformation-rate ratio for the Zagros Fold-and-Thrust collisional belt. *Geophysical Journal International*, *213*, 194–209. https://doi.org/10.1093/gji/ggx524
Payne, S., McCaffrey, R., & King, R. W. (2008). Strain-rates and contemporary deformation in the Snake river plain and surrounding Basin and range from GPS and seismicity. *Geology*, *36*(8), 647–650. https://doi.org/10.1130/G25039A.1
Pereira, R., & Alves, T. M. (2013). Crustal deformation and submarine canyon incision in a Meso-Cenozoic first-order transfer zone (SW Iberia, North Atlantic Ocean. *Tectonophysics*, *601*, 148–162. https://doi.org/10.1016/j.tecto.2013.05.007
Pinheiro, L., Wilson, R., Pena dos Reis, R., Whitmarsh, R., & Ribeiro, A. (1996). The western Iberian margin: A geophysical and geological overview. In R. Whitmarsh, D. Daywer, A. Klaus, & D. Masson (Eds.), *Proceedings of the Ocean Drilling Program, Leg 149, Scientific Results Volume* (pp. 533–545). IODP.
Ramalho, M., Matias, L., Neres, M., Carafa, M. M. C., Carvalho, A., & Costa, P. (2020). A sanity check for earthquake recurrence models used in PSHA of slow deforming regions: The case of SW Iberia. *Natural Hazards and Earth Systems Science Discussions*. https://doi.org/10.5194/nhess-2020-300
Rasmussen, E. ,S., Lomholt, S., Andersen, C., & Vejbæk, O. V. (1988). Aspects of the structural evolution of the Lusitanian Basin in Portugal and the shelf and slope area offshore Portugal. *Tectonophysics*, *300*, 199–225.
Reis, R., Pimentel, N., Fainstein, R., Reis, M., & Rasmussen, B. (2017). Influence of salt diapirism on the basin architecture and hydrocarbon prospects of the Western Iberian Margin. In J. Soto, J. Flinch, & G. Tari (Eds.), *Permo-triassic Salt Provinces of Europe, North Africa and the Atlantic Margins*. Elsevier. https://doi.org/10.1016/b978-0-12-809417-4.00015-x
Ribeiro, A., Cabral, J., Baptista, R., & Matias, L. (1996). Stress pattern in Portugal mainland and the adjacent Atlantic region, West Iberia. *Tectonics*, *15*, 641–659. https://doi.org/10.1029/95tc03683
Shen, Z.-K., Wang, M., Zeng, Y., & &Wang, F. (2015). Optimal interpolation of spatially discretized geodetic data. *Bulletin of Seismological Society of America*, *105*(4), 2117–2127. https://doi.org/10.1785/0120140247
Storchak, D. A., Harris, J., Brown, L., Lieser, K., Shumba, B., & Di Giacomo, D. (2020). Rebuild of the Bulletin of the International Seismological Centre (ISC)—Part 2: 1980–2010. *Geoscience Letters*, *7*, 18. https://doi.org/10.1186/s40562-020-00164-6
Stucchi, M., Rovida, A., Gómez, A., Alexandre, P., Camelbeeck, T., Demircioglu, M., et al. (2013). The SHARE European earthquake catalogue (SHEEC) 1000–1899. *Journal of Seismology*, *17*, 523–544. https://doi.org/10.1007/s10950-012-9335-2
Sylvester, A. G. (1988). Strike-slip faults. *GSA Bulletin*, *100*(11), 1666–1703. https://doi.org/10.1130/0016-7606(1988)100<1666:ssf>2.3.co;2
Vilanova, S. P., & Fonseca, J. F. B. D. (2004). Seismic hazard impact of the Lower Tagus Valley Fault Zone (SW Iberia), *Journal of Seismology*, *8*, 331–345.
Vilanova, S. P., & Fonseca, J. F. B. D. (2007). Probabilistic seismic-hazard assessment for Portugal. *Bulletin of the Seismological Society of America*, *97*, 1702–1717. https://doi.org/10.1785/0120050198
Walker, D. J. (1982). Final report: Seismic interpretation for Petrogal concession areas 45, 46, 47/48. GPEP.
Wang, H., Wright, T. J., Liu-Zeng, J., & Peng, L. (2019). Strain-rate distribution in south-central Tibet from two decades of InSAR and GPS. *Geophysical Research Letters*, *46*, 5170–5179. https://doi.org/10.1029/2019GL081916
Wegmuller, U., Werner, C., Magnard, C., & Manconi, A. (2019). *Co-seismic displacement vector retrieval for the Iran-Iraq Earthquake using Sentinel-1 (poster)*. ESA Living Planet Meeting Milano. Retrieved from https://www.gamma-rs.ch/uploads/media/2000-1_GAMMA_Software.pdf
Werner, C., Wegmuller, U., Strozzi, T., & Wiesman, A. (2000). *GAMMA SAR and Interferometric Software, ERS - ENVISAT Symposium* (pp. 16–20). Gothenburg, Sweden, Retrieved from https://www.gamma-rs.ch/uploads/media/2000-1_GAMMA_Software.pdf
Wessel, P., & Smith, W. H. F. (1991). Free software helps map and display data. *Eos Transactions American Geophysical Union*, *72*(41), 445–441. https://doi.org/10.1029/90EO00319
Wilson, R. C. L., Hiscott, R. N., Willis, M. G., & Gradstein, P. M. (1989). The Lusitanian Basin of west-central Portugal: Mesozoic and Tertiary tectonic, stratigraphic and subsidence history. In A. J. Tankard, & H. R. Balkwill (Eds.), *Extensional tectonics and stratigraphy of the North Atlantic margins* (Vol. 46, pp. 341–361). AAPG Memoir.
Woessner, J., Laurentiu, D., Giardini, D., Crowley, H., Cotton, F., Grünthal, G., et al. (2015). The 2013 European seismic hazard model: Key components and results. *Bulletin of Earthquake Engineering*, *13*(12), 3553–3596. https://doi.org/10.1007/s10518-015-9795-1
Youngs, R. R., & Coppersmith, K. J. (1985). Implications of fault slip rates and earthquake recurrence models to probabilistic seismic hazard estimates. *Bulletin of the Seismological Society of America*, *75*(4), 939–964.

References From the Supporting Information

Boehm, J., Werl, B., & Schuh, H. (2006). Troposphere mapping functions for GPS and very long baseline interferometry from European Centre for Medium-Range Weather Forecasts operational analysis data. *Journal of Geophysical Research: Solid Earth*, *111*, B02406. https://doi.org/10.1029/2005JB003629

Crosetto, M., Monserrat, O., Cuevas-González, M., Devanthéry, N., & Crippa, B. (2016). Persistent Scatterer Interferometry: A review. *ISPRS Journal of Photogrammetry and Remote Sensing*, *115*, 78–89. https://doi.org/10.1016/j.isprsjprs.2015.10.011.620778

Fujiwara, S., Nishimura, T., Murakami, M., Nakagawa, H., Tobita, M., & Rosen, A. P. (2000). 2.5-D surface deformation of M6.1 earthquake near Mt Iwate detected by SAR interferometry. *Geophysical Research Letters*, *70*(14), 2049–2052. https://doi.org/10.1029/1999gl011291

Petrie, E. J., King, M. A., Moore, P., & Lavallée, D. A. (2010). Higher-order ionospheric effects on the GPS reference frameand velocities. *Journal of Geophysical Research: Solid Earth*, *115*(B03417). https://doi.org/10.1029/2009JB006677